NeuroImage 202 (2019) 116123

Contents lists available at ScienceDirect

NeuroImage

journal homepage: www.elsevier.com/locate/neuroimage

# Vulnerability to mood degradation during sleep deprivation is influenced by white-matter compactness of the triple-network model

Sahil Bajaj *, William D.S. Killgore

*Social, Cognitive and Affective Neuroscience Laboratory, Department of Psychiatry, College of Medicine, University of Arizona, Tucson, AZ, USA*

ARTICLE INFO

*Keywords:*
Neuroimaging
Cortical structure
Default-mode network
Control-execution network
Salience network
Anisotropy
Cortical volume
Mean curvature
Grey/white matter

ABSTRACT

Sleep deprivation (SD) is often associated with significant shifts in mood state relative to baseline functioning. Prior work suggests that there are consistent trait-like differences among individuals in the degree to which their mood and performances are affected by sleep loss. The goal of this study was to determine the extent to which trait-like individual differences in vulnerability/resistance to mood degradation during a night of SD are dependent upon region-specific white and grey matter (WM/GM) characteristics of a *triple-network model*, including the default-mode network (DMN), control-execution network (CEN) and salience network (SN). Diffusion-weighted and anatomical brain data were collected from 45 healthy individuals several days prior to a 28-h overnight SD protocol. During SD, a visual analog mood scale was administered every hour from 19:15 (time point1; TP1) to 11:15 (TP17) the following morning to measure two positive and six negative mood states. Four core regions within the DMN, five within the CEN, and seven within the SN were used as regions of interest (ROIs). An index of mood resistance (IMR) was defined as the averaged differences between positive and negative mood states over 12 TPs (TP5 to TP16) relative to baseline (TP1 to TP4). For each ROI, characteristics of WM – quantitative anisotropy (QA) and mean curvature index (WM-MCI), and GM – cortical volume (CV) and GM-MCI were estimated, and used to predict IMR. WM characteristics, particularly QA, of all of regions within the DMN, and most of the regions within the CEN and SN predicted IMR during SD. In contrast, most ROIs did not show significant association between IMR and any of the GM characteristics (CV and MCI) or WM MCI. Our findings suggest that greater resilience to mood degradation induced by total SD appears to be associated with more compact axonal pathways within the DMN, CEN and SN.

## 1. Introduction

Sleep is a vital brain process that is necessary for normal cognitive, affective, social, and physical functioning (Beattie et al., 2015; Zielinski et al., 2016). While lack of sleep leads to obvious and well-established impairments in psychomotor vigilance, attention, and some aspects of cognition (Durmer and Dinges, 2005; Killgore, 2010), it also leads to time varying mood deterioration, particularly increases in state anxiety and stress, as well as lower scores on emotional intelligence, inter- and intrapersonal functioning, stress management skills, and reduced positive thinking (Killgore et al., 2008; Motomura et al., 2017; Schwarz et al., 2018). One to two nights of total sleep deprivation (SD) can lead to a weakening of prefrontal inhibitory systems, resulting in emotional dysregulation i.e., negative mood states and frustration (Killgore, 2010; Killgore et al., 2014; Kahn-Greene et al., 2006). Notably, several neuroimaging studies have suggested that SD can alter functional connectivity between the regulatory areas of the medial prefrontal cortex, a key node of the Default Mode Network (DMN), and the emotionally responsive regions of the limbic system, such as the amygdala (Motomura et al., 2017; Yoo et al., 2007; Simon et al., 2015; Feng et al., 2018; Shao et al., 2014; Killgore, 2013). A number of studies have now shown altered DMN connectivity during SD (De Havas et al., 2012; Yeo et al., 2015), and even normal variability in hours of sleep the night before a brain scan can affect the strength of this connectivity (Killgore et al., 2012). A recent graph theory study demonstrated that the global modularity of functional brain networks appears to decrease following SD, although there is an increase in limbic module density that correlates with increased emotional responsiveness (Ben Simon et al., 2017). Thus, the ability to regulate mood and emotional states appears to decline during SD (Goldstein and Walker, 2014), and this may be associated with altered network connectivity patterns within the emotion regulating areas of the brain, particularly the anterior DMN as well as emotionally relevant

* Corresponding author. 1501 N Campbell Avenue, Department of Psychiatry, Room # 7304B, University of Arizona, Tucson, AZ, 85724, USA.
*E-mail address:* sahil.neurores@gmail.com (S. Bajaj).

https://doi.org/10.1016/j.neuroimage.2019.116123
Received 18 February 2019; Received in revised form 15 July 2019; Accepted 23 August 2019
Available online 25 August 2019

systems such as the salience network (SN).

While cognitive and affective deficits have been well documented and reliably associated with SD, it is also true that lack of sleep does not affect all people to the same extent or in the same way (Tkachenko and Dinges, 2018). Work by Van Dongen and others has demonstrated that there are consistent trait-like differences in the magnitude of vulnerability/resistance that individuals show to cognitive declines during SD (Van Dongen et al., 2004, 2011, 2012; Van Dongen and Belenky, 2009; King et al., 2009; Patanaik et al., 2014; Rupp et al., 2012), and may involve networks such as the control-execution network (CEN). The specific cognitive or performance response to SD appears to be highly reproducible within a given individual even when assessed months or years apart (Dennis et al., 2017). Interestingly, these differences appear to be highly domain specific (i.e., affecting one type of cognitive ability but not another (Van Dongen et al., 2004)). Although less well studied, similar trait-like differences in vulnerability appear to be present for mood fluctuations during SD as well (Rupp et al., 2012).

While individual differences in vulnerability/resistance to the cognitive/performance effects of SD are highly reproducible within a given individual, it has proven difficult to find a reliable predictive marker of this phenomenon (Van Dongen and Belenky, 2009). Consequently, the underlying mechanisms that contribute to these individual differences remain largely unknown. Recently, there have been a number of brain imaging studies that have attempted to identify the neural correlates of vulnerability/resistance to SD. Initial studies focused on functional brain activation as a potential marker of this trait-like capacity (Yeo et al., 2015; Caldwell et al., 2005; Chee and Tan, 2010), while more recent studies have focused particularly on the integrity of WM axonal pathways (Cui et al., 2015; Rocklage et al., 2009). For instance, network-level functional connectivity analysis by Yeo and colleagues showed that highly connected and segregated brain networks become less integrated and segregated during SD (Yeo et al., 2015). Chee and colleagues reported that individuals who were vulnerable to SD had significantly reduced top-down fronto-parietal signal, particularly during SD attention lapses, whereas non-vulnerable individuals showed a trend towards greater top-down biasing of attention during SD lapses (Chee and Tan, 2010). Cui and colleagues reported that both functional responsiveness and microstructural features of the axonal connections i.e., structural integrity of specific axonal pathways within the fronto-parietal network were associated with individual differences in resistance to SD as defined by psychomotor vigilance performance (Cui et al., 2015).

Sleep deprivation not only affects vigilance and cognition, but also has a profound effect on emotion and mood (Killgore, 2010). While the functional and structural brain systems that contribute to vulnerability/resistance to vigilance and cognitive performance decrements during SD are beginning to be clarified, there is little known about the vulnerability/resistance factors that are associated with the degradation in mood that also occurs during SD. To our knowledge, there have been no published studies directly examining both grey and white-matter (GM/WM) neural predictive correlates of vulnerability to mood declines during SD. Previous studies reported strong negative associations between functional connectivity within the DMN and the levels of happiness (Luo et al., 2016), as well as between thoughts (described by words) during sad music, and ratings on mind-wandering – a core component of the DMN and greater centrality of the nodes within the DMN (Taruffi et al., 2017). Because of the strong established relationship between the DMN and mood, we expect that greater structural compactness, in terms of white and grey matter, within the regions comprising this network would be associated with greater capacity to modulate mood during SD. Moreover, the nodes within the CEN show strong co-activation during cognitively demanding tasks (Habas et al., 2009; Seeley et al., 2007), and the nodes within the SN constitute a network involved in processing interoceptive autonomic and emotional information (Seeley et al., 2007). Based on the intrinsic organization and functioning of the brain, a triple network model constituting these three networks, namely DMN, CEN and SN, was proposed to better understand the abnormal regulation of cognitive function in clinical neuroscience, including several major psychiatric and neurological disorders (Menon, 2011). It was also suggested that due to the impact of these networks on each other, the triple network model can be used to predict the dysfunction in psychopathology within a particular network from the other two networks (Menon, 2011).

In this study we investigated the characteristics of WM using some of the most advanced approaches for structural neuroimaging analysis, including quantitative anisotropy (QA) and white surface mean curvature index (MCI), and characteristics of GM including cortical volume (CV) and pial/grey surface MCI. Regarding WM diffusion parameters, we preferred to use water density measures such as QA rather than other diffusivity parameters such as fractional anisotropy (FA) or mean diffusivity, because QA is sensitive to density characteristics of WM, such as the compactness of the fiber bundles (Yeh et al., 2013, 2016a). It has also been found that compared to diffusivity measures, density measures are more sensitive to individual differences (Yeh et al., 2016a). Moreover, density measures such as QA are less susceptible to partial volume effects and are more capable of filtering out noisy values resulting in better tracking accuracy (Yeh et al., 2013). We hypothesized that individuals who have greater WM compactness i.e., greater QA, and thicker and larger cortex within the GM; i.e., CV for regions within the triple network model (DMN, CEN and SN) when measured up to a week before SD, would demonstrate greater resistance to mood degradation following a subsequent overnight session of SD relative to those who are more vulnerable to these shifts. Since thicker cortex is negatively associated with curvature i.e., local gyrification (Hogstrom et al., 2013), and greater cortical curvature is associated with WM atrophy (Deppe et al., 2014), we therefore also hypothesized that lesser WM/GM curvature would be associated with greater resistance to mood degradation in SD-individuals.

## 2. Materials and methods

### 2.1. Participants

Forty-five healthy individuals, who were between 20 and 43 years of age (mean age = 25.36 ± 5.62 years, 22 females) were recruited for this study. All of the participants were recruited from the greater Boston area, and were screened for any evidence of self-reported neurological, sleep, or medical disorders such as high/low blood pressure or symptoms related to stress or anxiety. All of the 45 participants were free of these medical issues according to self-report. All of the participants were native English speakers, and were found to be low to moderate users of alcohol (mean 4.7 ± 1.4 times per month) and caffeine (mean 67.41 ± 91.5 mg per day). Participants were excluded if they consumed excess alcohol (i.e., five or more alcoholic drinks per episode, or more than two drinks per day on average for the past two months for males, and more than four drinks per episode, or more than 1 drink per day on average for the past two months for females), or habitually consumed more than 300 mg of caffeine per day. Participants were also excluded for current use of marijuana or illicit substances. On the day of the scan, participants were asked to consume their normal morning caffeine to alleviate any withdrawal symptoms. None of the participants was a current smoker. All the participants provided written informed consent prior to data collection. The study protocol was approved by the Institutional Review Boards of McLean Hospital and the U.S. Army Human Research Protections Office.

### 2.2. Data collection

#### 2.2.1. Procedure

All participants were scheduled for three visits: baseline visit (V1), neuroimaging visit (V2), and sleep-deprivation visit (V3) to the lab. During V1, participants were informed of the study procedures and were also screened for the presence of any psychopathology using the Mini

International Neuropsychiatric Interview (MINI) (Sheehan et al., 1998) to confirm their eligibility for the study. After seven to ten days after V1, participants returned for V2 during which diffusion-tensor imaging (DTI) and T1-weighted data were collected from all the eligible participants. The goal was to use the V2 visit as a stable trait-like metric of brain structure that could potentially predict later resistance to sleep loss. Thus, one to four days after V2, participants returned for V3, during which they stayed awake overnight and a visual analog mood scale measure was collected every hour between 7:15 p.m. (TP1) and 11:15 a.m. (TP17) the following day (n = 17 time points) to measure 8 specific mood states (positive: happy and energetic, negative: tense, tired, angry, sad, afraid, confused). The two nights before V3, participants were instructed to go to bed between 10:00 and 11:00 p.m., remain in bed for 8 h each night before the SD visit, and abstain from any caffeine or other stimulants. Some behavioral, functional, and DTI data from the sample have been reported elsewhere (Cui et al., 2015), however, the associations between mood degradation, WM QA, and brain morphometry reported in this study are novel and have never been published.

#### 2.2.2. MRI session and scanning parameters

DTI and T1-weighted data were collected using a 3.0 T S Tim Trio scanner (Siemens, Erlangen, Germany). To control for circadian influences, most of the MRI sessions (96%) were consistently conducted within a 3-h time window, between 1:00 p.m. and 4:00 p.m. The mean clock time for collection of the T1-weighted scans, followed by diffusion-weighted scans, was 2:07 p.m. (±0.96 h). However, due to technical issues, two scans were performed before 1:00 p.m. (one at 11:00 a.m. and the other just after at 12:15 p.m.). Sleep diary and actigraphy (Actiwatch 2®; Philips Respironics) data showed that all of the participants had normal sleep quantity and quality prior to MRI session. Mean total sleep time (TST - minutes between sleep onset and wake time), and mean sleep efficiency (SE - percentage of time in bed that was scored as sleep) for the sample was 433.60 ± 58.62 min and 83.95 ± 7.23 percent respectively. Due to device failure, actigraphy data from five subjects were not recorded, therefore, SE statistics reported above are from 40 subjects. DTI data were collected using a single-shot echo-planar (gradient echo) imaging sequence with 40 transverse slices (FOV = 896 × 896 mm, acquisition matrix = 128 × 128, TR/TE = 6340 m s/99 m s, voxel size = 1.75 × 1.75 × 3.5 mm) encompassing the whole brain. Diffusion-weighted data were acquired along 72 directions with b = 1000 s/mm$^2$. A set of 8 images was acquired with no diffusion weighting (b = 0) images. DTI data from one participant were excluded due to poor image quality. T1-weighted magnetization-prepared rapid gradient-echo (MPRAGE) images were collected over 176 sagittal slices (TR/TE/flip angle = 2.1 s/2.25 m s/12°, 256 × 256 matrix) with voxel size = 1 × 1 × 1 mm.

#### 2.2.3. Visual analog mood scale (VAMS)

Mood states during the V3 (i.e., 28-h SD) session were evaluated using a set of modified visual analog mood scales (VAMS) (Monk, 1989; Folstein and Luria, 1973). The VAMS involved two items reflecting positive mood states (happiness and energy) and six items reflecting negative mood states (sadness, tension, fear, anger, confusion, and fatigue). In our current study, we used a modified version of the VAMS assessment technique described by Folstein and Luria (1973) and Monk, 1989, which uses verbal description to assess participant's mood (this should be differentiated from the commercially available VAMS product developed by Stern et al. (1997) (Stern et al., 1997), which uses schematic faces rather than verbal descriptors). Here participants had to rate their current mood using a vertical 100 mm line, anchored at each end by a descriptive statement. For example, for the happiness mood scale, participants rated their mood according to the verbal prompt saying, "How is your happiness right now?" ranging from "no happiness at all" or "neutral" at the bottom of the line versus "strongest happiness imaginable" on the top. Scores of each mood scale were determined by measuring the distance (in mm) from the bottom of the mood scale to the participants mark above.

### 2.3. Data analysis

#### 2.3.1. Regions of interest (ROIs)

Using spherical radius of 8 mm, four regions within the DMN (N1) – the posterior cingulate cortex (PCC) (N1R1), medial prefrontal cortex (MPFC) (N1R2), left and right lateral parietal cortices (L.LPC-1/R.LPC-1) (N1R3 and N1R4), five regions within the CEN (N2) – the dorsal medial prefrontal cortex (DMPFC) (N2R1), left and right anterior prefrontal cortex (L.APFC-1/R.APFC-1) (N2R2 and N2R3), left and right superior parietal cortex (L.SPC/R.SPC) (N2R4 and N2R5), and seven regions within the SN (N3) – the dorsal anterior cingulate cortex (DACC) (N3R1), left and right anterior prefrontal cortex (L.APFC-2/R.APFC-2) (N3R2 and N3R3), left and right insula (L.I/R.I) (N3R4 and N3R5) and left and right lateral parietal cortex (L.LPC-2/R.LPC-2) (N3R6 and N3R7) were used as ROIs for morphometric analysis. Peak MNI co-ordinates of each of the above ROIs (reported in Table 1) were based on previously published literature on resting-state brain connectivity (Raichle, 2011; Razi et al., 2017). For region-specific QA analysis, earlier defined ROIs were dilated by 4 mm to include WM. All of the ROIs within the DMN, CEN and SN are displayed on a diffusion-weighted image and surface-overlaid on T1-weighted images in Fig. 1 (DMN), Fig. 2 (CEN), and Fig. 3 (SN) respectively.

#### 2.3.2. DTI data

DTI data were converted from DICOM into NIFTI format using the dcm2nii function available in the MRIcron package (Rorden et al., 2007), which generated a *b*-value and *b*-vector file for each participant. For head-motion correction, standard eddy current correction was performed using the FMRIB Software Library v6.0 processing software package (https://fsl.fmrib.ox.ac.uk/fsl/fslwiki). The motion-corrected data were imported into DSI Studio (http://dsi-studio.labsolver.org). Data were further converted into SRC format, which stores the diffusion-weighted volumes, image dimensions, voxel size, and b-table. Each SRC file was thoroughly examined to ensure the quality and integrity of DTI data in terms of consistency of image dimensions, resolution, DWI count, and neighboring DWI correlation (NDC). No outlier in NDC values (greater than 3 median absolute deviation) was identified. Further, region specific QA was estimated from diffusion MRI group connectometry (Yeh et al., 2016b) using the Q-space diffeormophic reconstruction (QSDR) (Yeh and Tseng, 2011) approach implemented in DSI Studio. QSDR is a model-free approach, which calculates the distribution of water diffusion using a

**Table 1**
Abbreviations and peak-MNI co-ordinates of four regions within the DMN (N1) (N1R1, N1R2, N1R3 and N1R4), five regions within the CEN (N2) (N2R1, N2R2, N2R3, N2R4 and N2R5), and seven regions within the SN (N3) (N3R1, N3R2, N3R3, N3R4, N3R5, N3R6 and N3R7).

| # | Region | Abbreviation | MNI coordinates (X, Y, Z) |
|---|---|---|---|
| **N1** | **Network 1: Default-mode network (DMN)** | | |
| R1 | Posterior cingulate cortex/ Precuneus | PCC | 0, −52, 27 |
| R2 | Medial prefrontal cortex | MPFC | −1, 54, 27 |
| R3 | Left lateral parietal cortex | L.LPC-1 | −46, −66, 30 |
| R4 | Right lateral parietal cortex | R.LPC-1 | 49, −63, 33 |
| **N2** | **Network 2: Control-execution network (CEN)** | | |
| R1 | Dorsal medial prefrontal cortex | DMPFC | 0, 24, 46 |
| R2 | Left anterior prefrontal cortex | L.APFC-1 | −44, 45, 0 |
| R3 | Right anterior prefrontal cortex | R.APFC-1 | 44, 45, 0 |
| R4 | Left superior parietal cortex | L.SPC | −50, −51, 45 |
| R5 | Right superior parietal cortex | R.SPC | 50, −51, 45 |
| **N3** | **Network 3: Salience network (SN)** | | |
| R1 | Dorsal anterior cingulate cortex | DACC | 0, 21, 36 |
| R2 | Left anterior prefrontal cortex | L.APFC-2 | −35, 45, 30 |
| R3 | Right anterior prefrontal cortex | R.APFC-2 | 32, 45, 30 |
| R4 | Left insula | L.I | −41, 3, 6 |
| R5 | Right insula | R.I | 41, 3, 6 |
| R6 | Left lateral parietal cortex | L.LPC-2 | −62, −45, 30 |
| R7 | Right lateral parietal cortex | R.LPC-2 | 62, −45, 30 |

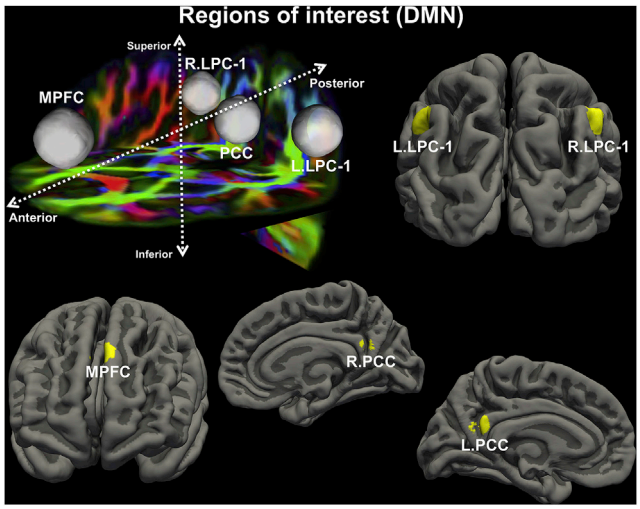


**Fig. 1. ROIs within the DMN.** Here we show ROIs within the DMN overlaid on 3D diffusion-weighted image and surface-map of standard anatomical image.

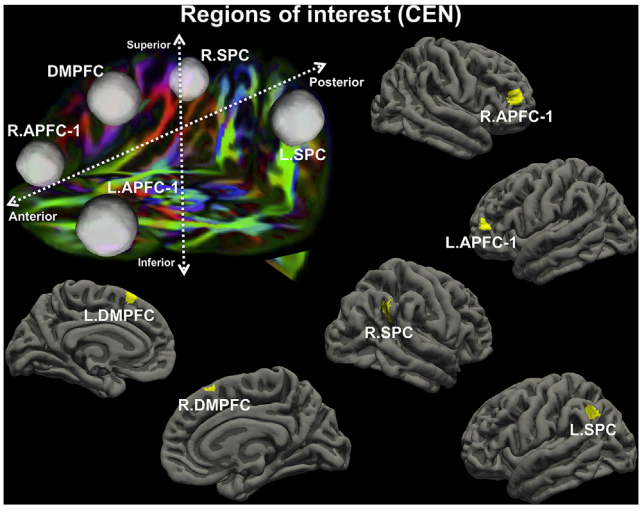


**Fig. 2. ROIs within the CEN.** Here we show ROIs within the CEN overlaid on 3D diffusion-weighted image and surface-map of standard anatomical image.

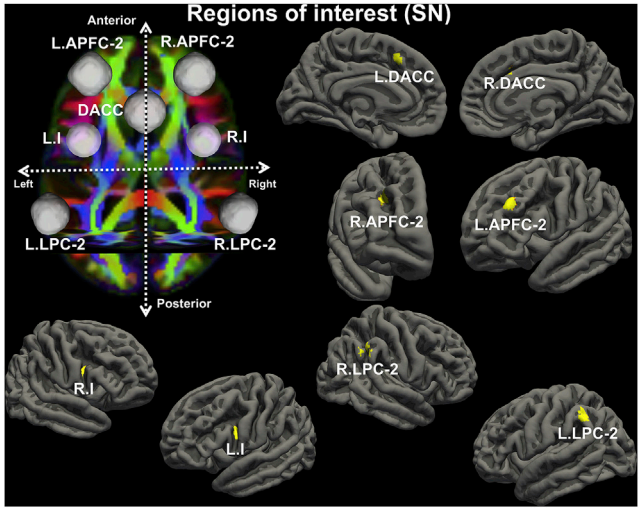


**Fig. 3. ROIs within the SN.** Here we show ROIs within the SN overlaid on 3D diffusion-weighted image and surface-map of standard anatomical image.

high-resolution standard brain atlas constructed from 90-diffusion spectrum imaging datasets in the ICBM-152 space. Automated registration to standard template space was used for each participant. A subject-averaged map of raw QA was computed in standard MNI-space (Fig. 4A). Therefore, all the ROIs were defined in standard MNI space in order to extract QA-values from diffusion MRI connectometry in QSDR-space.

### 2.3.3. Anatomical data

We used the standard "recon-all" pipeline in FreeSurfer 6.0.0 (https://surfer.nmr.mgh.harvard.edu) to process the T1-weighted data. The preprocessing steps included intensity normalization, removal of non-brain tissue, automated transformation to the standard MNI co-ordinate system, volumetric segmentation into cortical and sub-cortical matter, and cortical segmentation of the cerebral cortex (Desikan et al., 2006). Standard quality control steps involved a careful visual inspection of skull-stripped brain volumes, masks, and pial surfaces. Several morphometry measures, *including* cortical thickness (CT) (Fischl and Dale, 2000), cortical surface area (CSA) (Fischl et al., 1999), and cortical volume (CV) (Winkler et al., 2018), for each of the ROIs were estimated. However, since CV already accounts for both CT and CSA (Winkler et al., 2010, 2018), we therefore, only report measures of CV in this study. Mean curvature index (MCI), which is more susceptible to geometric changes of cortical surface, has also been widely used to better understand the complexity of cortical folds (Im et al., 2008), and is also reported in our current study. By definition, MCI is a local measure of the degree of folding of a surface. For each ROI, MCI was also estimated from both pial and white surfaces. Here, we used pial surface (outer boundary of the GM), as its more sensitive to GM atrophy, and white-surface (boundary between GM and WM, or outer boundary of the WM), as its insensitive to GM atrophy but more sensitive to WM atrophy. Previously, measures of cortical folding in terms of mean curvature have been extensively used to quantify the complexity of brain folds (Deppe et al., 2014; Im et al., 2008; Batchelor et al., 2002). It has also been found that due to high spatial frequency the curvature indices such MCIs (i.e., millimeter scale measures of intrinsic curvature) are more sensitive and reliable measures to quantify cortical gyrification as compared to gyrification indices such as local gyrification indices (i.e., centimeter-scale extrinsic measures) (Ronan et al., 2012). Higher MCI values (positive or negative) represent sharper curves, where positive MCIs correspond to curvatures pointing "up" i.e., sulci, and negative MCIs correspond to curvatures pointing "down" i.e., gyri. FreeSurfer estimates the morphometry measures separately for the left and right hemisphere. Two of our ROIs (PCC and MPFC) of the DMN, one ROI (DMPFC) of the CEN, and one ROI (DACC) of the SN lie at the midline sharing their vertices bilaterally (i.e., present in both hemispheres), therefore, morphometry measures for these ROIs (i.e., left PCC (L.PCC), right PCC (R.PCC), left MPFC (L.MPFC), right MPFC (R.MPFC), left DMPFC (L.DMPFC), right DMPFC (R.DMPFC), left DACC (L.DACC), and right DACC (R.DACC)) were estimated separately for each hemisphere. Furthermore, subject-averaged vertex-wise maps of white-matter MCI (WM-MCI) (Fig. 4B), CV (Fig. 4C), and grey-matter MCI (GM-MCI) (Fig. 4D) were computed in standard MNI space. Group-average values for each of these measures (QA, WM-MCI, CV and GM-MCI) for each ROI are reported in Table 2.

### 2.3.4. Index of mood resistance

Previously, Cui and colleagues defined *percent reaction speed change (PRSC)* (Cui et al., 2015) as a metric to evaluate resistance to SD as: PRSC = ((reaction speed from 12 a.m. to 11 a.m.)/(reaction speed from 7 p.m. to 11 p.m.)) × 100%. Similarly, we defined the index of mood resistance (IMR) as a metric to evaluate resistance to mood degradation following SD as: IMR = ((mood states from 11:15 p.m. to 10:15 a.m.)/(mood states from 7:15 p.m. to 10:15 p.m.)) × 100%. More specifically, IMR (in percentage), or mood degradation (equation (1)), was estimated by averaging scores on six negative (N) mood scales (N1 to N6) over 12 TPs

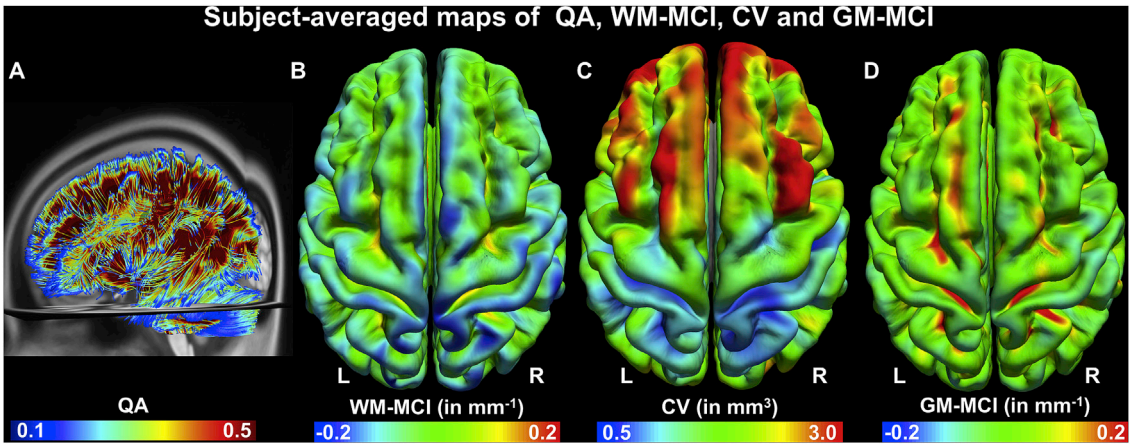


**Fig. 4. Subject-averaged maps of QA and characteristics of WM and GM.** Here we show whole brain subject averaged 3D-maps of (A) QA estimated from diffusion connectometry analysis, (B) vertex-wise WM-MCI, (C) vertex-wise CV, and (D) vertex-wise GM-MCI in standard MNI space.

**Table 2**
Group-average values for QA, WM-MCI, CV and GM-MCI for each regions of interest.

| # | Region | Mean (Standard Deviation) | | | |
|---|---|---|---|---|---|
| | | QA | WM-MCI ($mm^{-1}$) | CV ($mm^3$) | GM-MCI ($mm^{-1}$) |
| N1 | **Network 1: Default-mode network (DMN)** | | | | |
| R1 | PCC | 0.14 (0.03) | −0.05 (0.01) | 1.72 (0.23) | −0.005 (0.01) |
| R2 | MPFC | 0.15 (0.03) | −0.10 (0.01) | 2.73 (0.29) | −0.02 (0.02) |
| R3 | L.LPC-1 | 0.23 (0.05) | −0.06 (0.02) | 1.95 (0.39) | 0.01 (0.02) |
| R4 | R.LPC-1 | 0.20 (0.04) | −0.06 (0.02) | 2.02 (0.39) | 0.004 (0.04) |
| **N2** | **Network 2: Control-execution network (CEN)** | | | | |
| R1 | DMPFC | 0.14 (0.02) | −0.09 (0.02) | 2.35 (0.28) | −0.01 (0.02) |
| R2 | L.APFC-1 | 0.23 (0.04) | −0.01 (0.01) | 2.63 (0.46) | 0.05 (0.03) |
| R3 | R.APFC-1 | 0.18 (0.04) | −0.01 (0.01) | 2.32 (0.36) | 0.06 (0.02) |
| R4 | L.SPC | 0.17 (0.04) | −0.01 (0.002) | 1.60 (0.13) | 0.04 (0.005) |
| R5 | R.SPC | 0.19 (0.04) | −0.01 (0.003) | 1.61 (0.13) | 0.04 (0.005) |
| **N3** | **Network 3: Salience network (SN)** | | | | |
| R1 | DACC | 0.14 (0.03) | −0.01 (0.002) | 1.82 (0.17) | 0.05 (0.02) |
| R2 | L.APFC-2 | 0.15 (0.03) | −0.01 (0.002) | 1.60 (0.13) | 0.04 (0.005) |
| R3 | R.APFC-2 | 0.17 (0.04) | 0.004 (0.02) | 2.23 (0.47) | 0.07 (0.03) |
| R4 | L.I | 0.26 (0.05) | 0.04 (0.01) | 1.12 (0.16) | 0.10 (0.02) |
| R5 | R.I | 0.23 (0.04) | 0.06 (0.01) | 1.03 (0.13) | 0.11 (0.02) |
| R6 | L.LPC-2 | 0.14 (0.03) | −0.08 (0.03) | 1.75 (0.40) | 0.004 (0.03) |
| R7 | R.LPC-2 | 0.15 (0.03) | −0.05 (0.02) | 2.06 (0.33) | 0.02 (0.03) |

(from TP5 to TP16), subtracting this from the averaged score on two positive (P) mood scales (P1 and P2) over the same 12 TPs (equations (2) and (3)), and further dividing this by the averaged difference at the baseline (from TP1 to TP4) (equation (4)) as following:

$$IMR = \frac{P_{AV} - N_{AV}}{PN_{AVB}} \times 100 \quad (1)$$

where

$$P_{AV} = \frac{\sum_{t=5}^{16} \left( \frac{P1+P2}{2} \right)_t}{12}, \quad (2)$$

$$N_{AV} = \frac{\sum_{t=5}^{16} \left( \frac{N1+N2+N3+N4+N5+N6}{6} \right)_t}{12} \quad (3)$$

and

$$PN_{AVB} = P_{AVB} - N_{AVB} \quad (4)$$

Here, $P_{AV}$, $N_{AV}$ *and* $PN_{AVB}$ represent the average of average positive mood states over 12 time-points (TP5 to TP16, represented by $t = 5$ to 16), the average of negative mood states over the same 12 time-points (TP5 to TP16), and the difference between the average of positive and the average of negative mood states over first four baseline time-points (TP1 to TP4, represented by $t = 1$ to 4) respectively. Here, the average of positive (equation (5)) and the average of negative mood states (equation (6)) over the first four baseline time-points is calculated as following:

$$P_{AVB} = \frac{\sum_{t=1}^{4} \left( \frac{P1+P2}{2} \right)_t}{4} \quad (5)$$

and

$$N_{AVB} = \frac{\sum_{t=1}^{4} \left( \frac{N1+N2+N3+N4+N5+N6}{6} \right)_t}{4} \quad (6)$$

Data from first four time-points (7:15 p.m., 8:15 p.m., 9:15 p.m. and 10:15 p.m.) were included to determine the baseline mood because these all occur prior to 11:00 p.m., which is often the point where appreciable declines in vigilance become apparent following a normal day of wakefulness (Wesensten et al., 2005). In addition, data from the last TP (i.e., TP17 at 11:15 a.m.) was not included in the analysis, as this final time point was influenced significantly by anticipation of the end of the study. Overall, four IMR data points (i.e., data from four subjects) were identified as extreme outliers (i.e., with a value more than 3.0 inter-quartile range above/below the upper/lower quartile), and were excluded from the analysis. Thus, the IMR can be conceptualized as an index that describes how resistant an individual's mood is to the degrading effects of SD. Lower values represent greater vulnerability to the effects of sleep loss on mood, while higher values represent greater resistance capacity.

### 2.3.5. Correlation analysis

'Age, 'sex', and 'scores on the morningness-eveningness questionnaire

(MEQ)' (Horne and Ostberg, 1976) were used as covariates to estimate the partial correlation coefficients between IMR and characteristics of WM (QA and WM-MCI) and GM (CV and GM-MCI). Total intracranial volume was used as an additional covariate for estimating partial correlation coefficients between IMR and CV, and mean CT of the whole-brain was used as an additional covariate for estimating partial correlation coefficients between IMR and MCIs (WM and GM). In Supplementary Table 1, we also report the partial correlation coefficients between IMR and CT (age, sex, MEQ and mean CT as covariates), as well as between IMR and CSA (age, sex, MEQ and ICV as covariates). Data points with Cook's distance of more than 3 times the mean were considered as outliers, and were excluded from the analysis on a region-by-region basis.

## 3. Results

### 3.1. Mood degradation and WM characteristics

#### 3.1.1. Mood degradation and WM QA

Partial correlation analysis was performed between IMR and region-specific QA-values for all of the ROIs within each network.

*IMR and QA within the DMN:* We found significant positive associations between IMR and QA of all of the ROIs within the DMN - PCC ($r = 0.47$, $p = 0.048$) (Fig. 5A), MPFC ($r = 0.48$, $p = 0.039$) (Fig. 5B), L.LPC-1 ($r = 0.57$, $p = 0.006$) (Fig. 5C), and R.LPC-1 ($r = 0.52$, $p = 0.015$) (Fig. 5D). P-values reported here are adjusted p-values after Bonferroni-Holm correction. In Fig. 5, the correlations denoted with '**' represent significant correlations after Bonferroni-Holm correction.

*IMR and QA within the CEN:* Partial correlation analysis between IMR and QA for each ROI within the CEN (Fig. 6A–E) showed that there was significant positive associations between IMR and QA for R.APFC-1 ($r = 0.45$, $p = 0.05$) (Fig. 6C) and R.SPC ($r = 0.50$, $p = 0.028$) (Fig. 6E). However, other ROIs did not show significant associations between IMR and QA: DMPFC ($r = 0.34$, $p = 0.200$) (Fig. 6A), L.APFC-1 ($r = 0.29$, $p = 0.243$) (Fig. 6B) and L.SPC ($r = 0.35$, $p = 0.240$) (Fig. 6D). P-values reported here are adjusted p-values after Bonferroni-Holm correction. In Fig. 6, the 'dotted' sub-plots represent the non-significant associations between IMR and QA. The correlations denoted with '* and '**' represent significant correlations before and after Bonferroni-Holm correction respectively.

*IMR and QA within the SN:* Partial correlation analysis between IMR and QA for each ROI within the SN (Fig. 7A–G) showed that there were significant positive associations between IMR and QA for R.APFC-2 ($r = 0.46$, $p = 0.048$) (Fig. 7C) and R.LPC-2 ($r = 0.46$, $p = 0.05$) (Fig. 7G). However, other ROIs did not show significant associations between IMR and QA: DACC ($r = 0.36$, $p = 0.24$) (Fig. 7A), L. APFC-2 ($r = 0.24$, $p = 0.178$) (Fig. 7B), L.I ($r = 0.34$, $p = 0.204$) (Fig. 7D), R.I ($r = 0.35$, $p = 0.238$) (Fig. 7E) and L.LPC-2 ($r = 0.28$, $p = 0.243$) (Fig. 7F). P-values reported here are adjusted p-values after Bonferroni-Holm correction. In Fig. 7, the 'dotted' sub-plots represent the non-significant associations between IMR and QA. The correlations denoted with '* and '**' represent significant correlations before and after Bonferroni-Holm correction respectively.

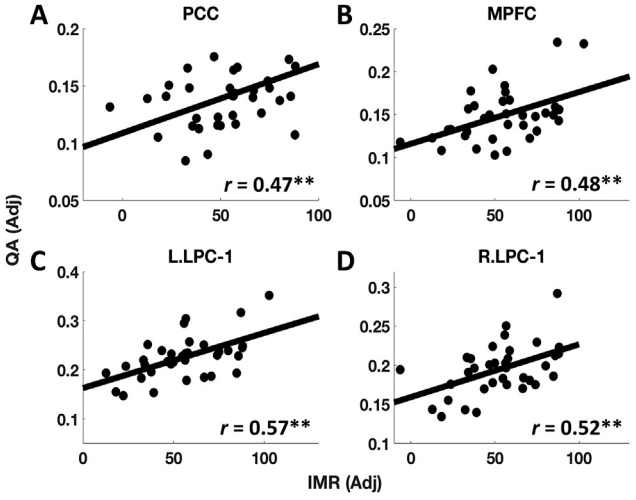


**Fig. 5. Association between adjusted IMR and adjusted QA of the DMN.** Here we show scatter plots for associations observed between IMR and QA for (A) PCC, (B) MPFC, (C) L.LPC-1, and (D) R.LPC-1. The correlations denoted with '**' represent significant correlations after Bonferroni-Holm correction.

#### 3.1.2. Mood degradation and WM-MCI

Partial correlation analysis between IMR and region-specific WM-MCI showed that there was no significant association between IMR and WM-MCI for any of the ROIs for any network (after Bonferroni-Holm correction).

The preceding findings (3.1.1 and 3.1.2), along with confidence intervals at 95% level and both non-adjusted and adjusted p-values (after Bonferroni-Holm correction) are summarized in Table 3.

### 3.2. Mood degradation and GM characteristics

Partial correlation analysis between IMR and CV showed that there was no significant association between IMR and CV for any of the ROIs for DMN (Fig. 8), CEN (Fig. 9), or SN (Fig. 10). In Figs. 8–10, the 'dotted' sub-plots represent the non-significant associations between IMR and CV. Also, there was no significant association between IMR and GM-MCI for any of the ROIs for any network. These findings between IMR and GM characteristics (CV and GM-MCI) are summarized in Table 3.

### 3.3. Association between WM-MCI and GM-MCI

Several of the ROIs, except MPFC within the DMN, R.APFC-1 and bilateral SPC (L.SPC and R.SPC) within the CEN, and DACC, L.APFC-2 and bilateral insula (L.I and R.I) within the SN, showed significant positive association between WM-MCI and GM-MCI (after Bonferroni-Holm correction). These findings, along with confidence intervals at 95% level and both non-adjusted and adjusted p-values (after Bonferroni-Holm correction) are summarized in Table 4.

## 4. Discussion

In this study we investigated the associations between structural aspects of WM/GM - collected at an independent time and measures of mood stability/resistance collected several days later during a period of overnight SD. Prior research suggests that there are consistent trait-like individual differences in the ability to resist SD. These effects may be specific to particular cognitive domains across individuals (Van Dongen et al., 2004), but this has never been extended to the ability to sustain mood during prolonged wakefulness. In accordance with our a priori hypothesis, our findings suggest that greater compactness within the WM of the triple network model, constituting all of the ROIs within the DMN and some of the ROIs within the CEN and SN, is associated with greater ability to sustain mood shifts induced by SD, even when tested several days after brain imaging. However, contrary to our hypothesis, we did not find any association between characteristics of GM and ability to sustain mood shifts induced by SD. Thus, we find that individuals with the greatest WM compactness at baseline testing were relatively stable and unaffected in their mood state during an overnight period of subsequent sleep loss, while those with less compactness of WM were more vulnerable to mood declines during the overnight SD period. Interestingly, contrary to our a priori hypothesis, structural characteristics of GM within any network, regardless of sub-region, were not predictive of the later ability to resist mood shifts due to SD. In particular, it could be due to strong correlations between curvature indices of WM and GM for

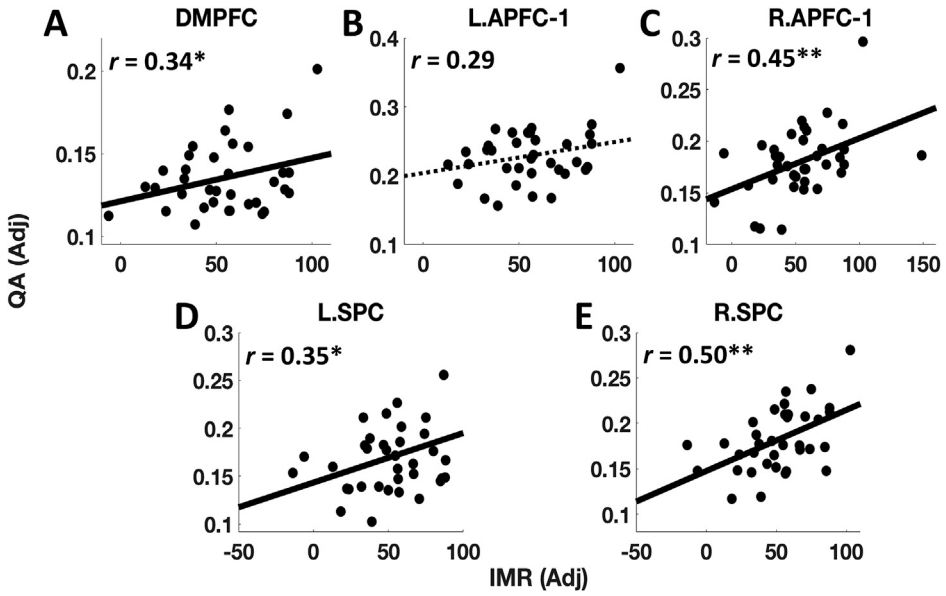


**Fig. 6. Association between adjusted IMR and adjusted QA of the CEN.** Here we show scatter plots for associations observed between IMR and QA for (A) DMPFC, (B) L-APFC-1, (C) R.APFC-1, (D) L.SPC, and (E) R.SPC. The 'dotted' sub-plots represent the non-significant associations between IMR and QA. The correlations denoted with '* and '**' represent significant correlations before and after Bonferroni-Holm correction respectively.

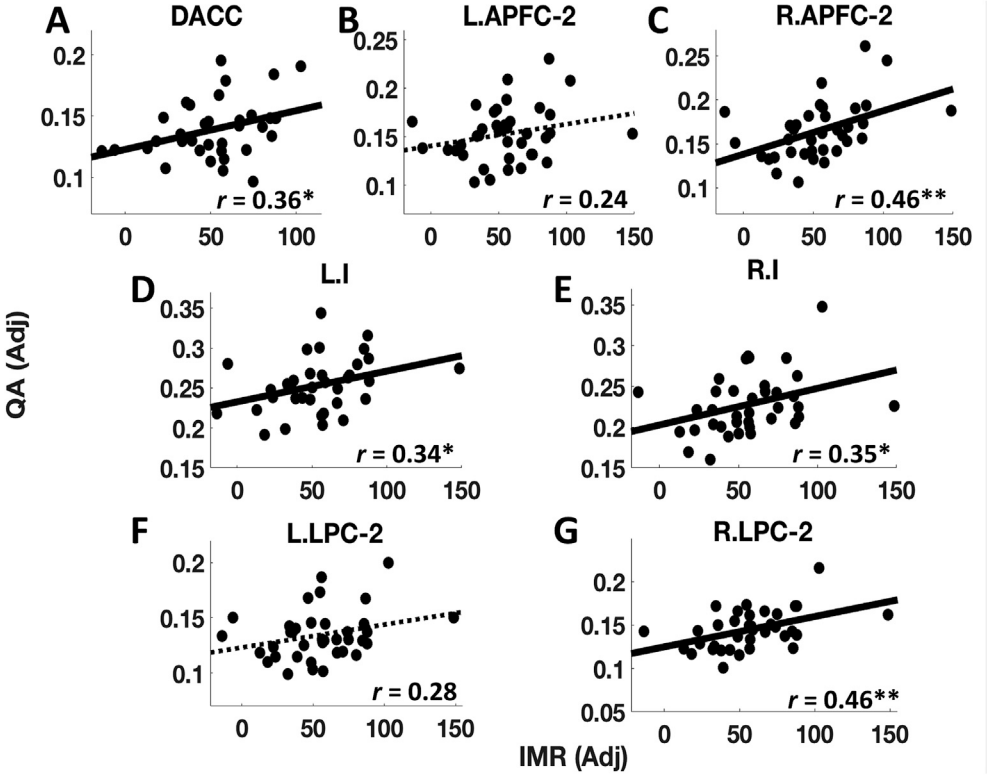


**Fig. 7. Association between adjusted IMR and adjusted QA of the SN.** Here we show scatter plots for associations observed between IMR and QA for (A) DACC, (B) L-APFC-2, (C) R.APFC-2, (D) L.I, (E) R.I, (F) L.LPC-2, and (G) R.LPC-2. The 'dotted' sub-plots represent the non-significant associations between IMR and QA. The correlations denoted with '* and '**' represent significant correlations before and after Bonferroni-Holm correction respectively.

several regions, that none of the MCIs (either WM or GM) showed an association with mood degradation induced by sleep loss. However, it is important to mention here that greater cortical curvature i.e., greater gyrification, has been previously reported to be associated with WM atrophy (Deppe et al., 2014), although all of the participants in our study were young adults who were screened extensively for health conditions. Nonetheless, we find that relatively increased WM compactness for most of the ROIs within the triple-network model is associated with greater resistance to mood disruption during sleep loss.

We found that for all of the regions within the DMN and several of the regions within the CEN and SN, the associations between QA and IMR were significant after Bonferroni-Holm correction. Our findings are in

**Table 3**
Summary for the relationships between IMR and characteristics of WM (QA and WM-MCI) and GM (CV and GM-MCI).

| Regions | | Relationships *between* IMR and | | | |
|---|---|---|---|---|---|
| | | White-matter (WM) | | Grey-matter (GM) | |
| | | **QA *(r, p, p1)* [CI]** | **WM-MCI *(r, p)* [CI]** | **CV *(r, p)* [CI]** | **GM-MCI *(r, p)* [CI]** |
| ***N1: DMN*** | | | | | |
| N1R1 | PCC | 0.47, **0.004***, **0.048**** [0.16, 0.69] | −0.06, 0.73 [-0.37, 0.27] | 0.11, 0.51 [-0.22, 0.41] | −0.03, 0.83 [-0.35, 0.28] |
| N1R2 | MPFC | 0.48, **0.003***, **0.039**** [0.17, 0.70] | 0.20, 0.22 [-0.12, 0.49] | −0.01, 0.93 [-0.33, 0.30] | 0.16, 0.35 [-0.18, 0.46] |
| N1R3 | L.LPC-1 | 0.57, **0.0004***, **0.006**** [0.29, 0.76] | 0.15, 0.36 [-0.17, 0.45] | 0.23, 0.17 [-0.10, 0.52] | 0.09, 0.60 [-0.24, 0.40] |
| N1R4 | R.LPC-1 | 0.52, **0.001***, **0.015**** [0.24, 0.73] | 0.05, 0.77 [-0.28, 0.37] | 0.17, 0.29 [-0.15, 0.46] | 0.11, 0.50 [-0.21, 0.42] |
| ***N2: CEN*** | | | | | |
| N2R1 | DMPFC | 0.34, **0.043***, 0.200 [0.01, 0.60] | 0.01, 0.95 [-0.31, 0.33] | 0.19, 0.24 [-0.13, 0.48] | −0.01, 0.94 [-0.33, 0.30] |
| N2R2 | L.APFC-1 | 0.29, 0.081, 0.243 [-0.04, 0.57] | −0.01, 0.97 [-0.33, 0.32] | −0.03, 0.84 [-0.35, 0.29] | 0.05, 0.75 [-0.27, 0.37] |
| N2R3 | R.APFC-1 | 0.45, **0.005***, **0.050**** [0.15, 0.67] | −0.18, 0.28 [-0.48, 0.15] | 0.18, 0.27 [-0.14, 0.47] | −0.18, 0.27 [-0.47, 0.14] |
| N2R4 | L.SPC | 0.35, **0.034***, 0.240 [0.03, 0.61] | 0.002, 0.99 [-0.32, 0.32] | 0.19, 0.27 [-0.15, 0.48] | 0.11, 0.50 [-0.22, 0.42] |
| N2R5 | R.SPC | 0.50, **0.002***, **0.028**** [0.21, 0.71] | −0.17, 0.31 [-0.46, 0.16] | 0.16, 0.33 [-0.16, 0.46] | −0.002, 0.99 [-0.32, 0.32] |
| ***N3: SN*** | | | | | |
| N3R1 | DACC | 0.36, **0.030***, 0.240 [0.04, 0.62] | −0.09, 0.59 [-0.40, 0.24] | 0.17, 0.30 [-0.16, 0.47] | −0.17, 0.32 [-0.47, 0.17] |
| N3R2 | L.APFC-2 | 0.24, 0.145, 0.178 [-0.08, 0.52] | 0.006, 0.97 [-0.31, 0.32] | 0.19, 0.27 [-0.15, 0.48] | 0.11, 0.51 [-0.22, 0.42] |
| N3R3 | R.APFC-2 | 0.46, **0.004***, **0.048**** [0.16, 0.69] | −0.13, 0.45 [-0.43, 0.20] | 0.22, 0.18 [-0.11, 0.51] | −0.12, 0.47 [-0.42, 0.20] |
| N3R4 | L.I | 0.34, **0.040***, 0.204 [0.02, 0.60] | 0.28, 0.08 [-0.04, 0.55] | 0.00, 0.99 [-0.32, 0.32] | 0.27, 0.11 [-0.06, 0.54] |
| N3R5 | R.I | 0.35, **0.034***, 0.238 [0.03, 0.60] | −0.10, 0.55 [-0.41, 0.23] | −0.03, 0.87 [-0.34, 0.29] | −0.18, 0.27 [-0.47, 0.14] |
| N3R6 | L.LPC-2 | 0.28, 0.089, 0.243 [-0.04, 0.56] | −0.02, 0.89 [-0.34, 0.30] | −0.09, 0.60 [-0.40, 0.24] | 0.17, 0.31 [-0.16, 0.47] |
| N3R7 | R.LPC-2 | 0.46, **0.005***, **0.050**** [0.15, 0.68] | 0.42, **0.01***, 0.07 [0.11, 0.66] | 0.10, 0.57 [-0.23, 0.41] | 0.16, 0.33 [-0.17, 0.46] |

*significant at $p \leq 0.05$.
**significant at $p1 \leq 0.05$ (adjusted p-values after Bonferroni-Holm correction).
[CI] represents confidence intervals at 95% level.

line with several previous reports, and also further clarify the structural role of regions involved in the triple-network model in mood sustainment during sleep loss. Importantly, SD had been reliably shown to lead to disrupted mood regulation (Penetar et al., 1993; Tempesta et al., 2010). Goldstein and colleagues extensively reviewed the relationships between brain function and emotional processing abnormalities caused by SD (Goldstein and Walker, 2014). Without adequate sleep, the brain is not able to process through emotional information effectively, affective

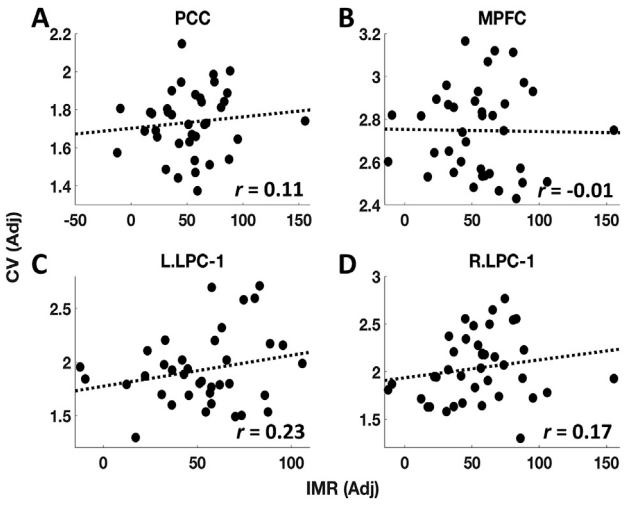


**Fig. 8. Non-significant associations between adjusted IMR and adjusted CV of the DMN.** Here we show scatter plots for associations observed between IMR and CV for (A) PCC, (B) MPFC, (C) L.LPC-1, and (D) R.LPC-1.

homeostasis is disrupted, and events become tagged as more emotionally intense than they would be following a night of normal sleep. Relevant to our findings about the DMN and SN, it was previously found that a single night of sleep loss may reduce functional connectivity between the medial prefrontal cortex and the amygdala in response to emotionally negative images, compared to a normal night of sleep (Yoo et al., 2007). Killgore also demonstrated that insufficient sleep prior to scanning was associated with altered functional connectivity between the ventromedial prefrontal cortex and amygdala (Killgore, 2013). In a recent review, Killgore and colleagues also discussed the role of prefrontal regions in emotional regulation during SD, suggesting that individuals who are sleep deprived tend to be more inclined towards negative mood i.e., more irritable, less happy, and less empathic, due to altered functional connectivity between prefrontal cortex and limbic network (Killgore et al., 2014). Moreover, during verbal learning tasks, both bilateral parietal cortices and regions within the frontal lobe activate more extensively following SD than in the rested condition (Drummond et al., 2000), suggesting compensatory recruitment of resources during prolonged wakefulness. Moreover, a recent functional connectivity study showed that sleep deprivation leads to a dissociation of DMN regions, leading to a reduced involvement of dorsal systems in cognition and behavioral control, and an increase in ventral DMN systems involved in emotional responsiveness (Chen et al., 2018). Thus, SD affects functional connectivity between the DMN, CEN, and emotional processing regions of the brain, a finding that is further strengthened by the present findings of greater structural integrity within the triple-network system among individuals who later demonstrate the greatest resistance to the effects of SD on mood. These findings suggest that these brain characteristics may represent a consistent trait-like feature that is associated with resistance to mood degradation during periods of insufficient sleep.

Prior work has shown that WM integrity, particularly as indexed by FA, is associated with the ability to resist the adverse effects of SD on some cognitive processes. For instance, Rocklage and colleagues reported that individual differences in WM organization are associated with susceptibility to cognitive performance deficits following total SD over a 24-h session (Rocklage et al., 2009). Greater baseline activation within the parietal and frontal regions and greater FA for tracts connecting the two areas have also been reported to be associated with greater resistance to SD – measured through faster speed of performance on the psychomotor vigilance test (PVT) (Cui et al., 2015). It has been found that among several factors, including the density and orientation of axons, the degree of myelination and diameter of axons may influence WM anisotropy measures (Beaulieu, 2002), which likely contributes to response speed

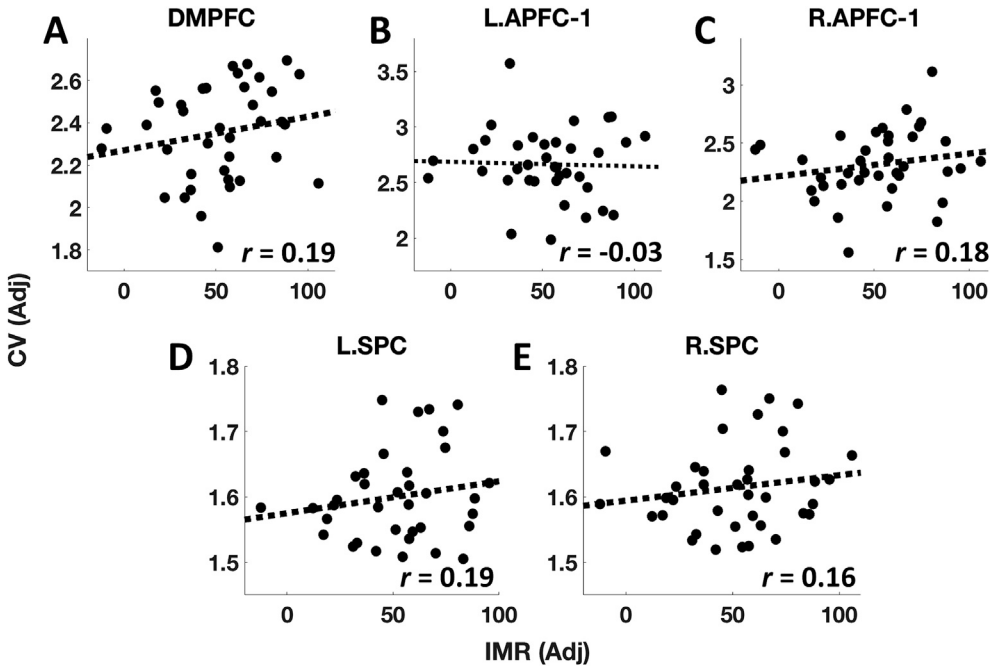


**Fig. 9. Non-significant associations between adjusted IMR and adjusted CV of the CEN.** Here we show scatter plots for associations observed between IMR and CV for (A) DMPFC, (B) L-APFC-1, (C) R.APFC-1, (D) L.SPC, and (E) R.SPC.

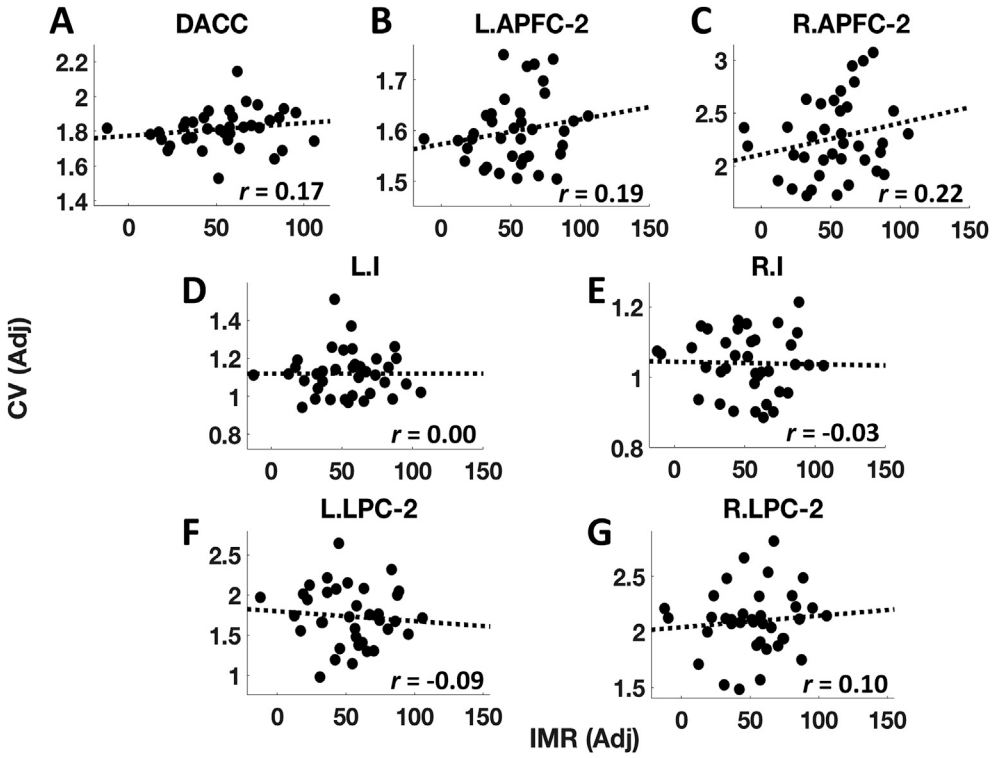


**Fig. 10. Non-significant associations between adjusted IMR and adjusted CV of the SN.** Here we show scatter plots for associations observed between IMR and CV for (A) DACC, (B) L-APFC-2, (C) R.APFC-2, (D) L.I, (E) R.I, (F) L.LPC-2, and (G) R.LPC-2.

during SD. Tuch and colleagues discussed several underlying potential mechanisms responsible for the potential role of WM in modulating and strengthening cognitive abilities. First, differences in WM physiology i.e., greater myelin thickness may cause greater FA and nerve conduction velocity (Jack et al., 1983). In other words, a higher degree of myelination may contribute to faster conduction and response speed on the PVT, but in the same vein, may also contribute to better mood resistance to SD due to faster and more efficient signal transmission within the fronto-parietal and fronto-limbic networks or with other emotion regulation regions. Second, individual differences in axon diameter may also contribute to faster nerve conduction velocity (Jack et al., 1983; Tuch et al., 2005). The widespread development of cortical pathways in terms of greater WM diffusivity, may influence an individual's capacity to sustain performance during SD (Rocklage et al., 2009). It has also been

**Table 4**
Summary for the relationships between characteristics of WM (WM-MCI) and GM (GM-MCI).

| Regions | | Relationships *between* WM-MCIs and GM-MCIs *(r, p, p1)* [CI] |
|---|---|---|
| ***N1: DMN*** | | |
| N1R1 | PCC | 0.52, **0.001***, **0.009**** [0.23 0.72] |
| N1R2 | MPFC | 0.41, **0.009***, 0.072 [0.11 0.64] |
| N1R3 | L.LPC-1 | 0.59, **0.0001***, **0.001**** [0.34 0.77] |
| N1R4 | R.LPC-1 | 0.54, **0.0003***, **0.003**** [0.28 0.73] |
| ***N2: CEN*** | | |
| N2R1 | DMPFC | 0.77, **0.000***, **0.00**** [0.59 0.88] |
| N2R2 | L.APFC-1 | 0.55, **0.0003***, **0.003**** [0.28 0.74] |
| N2R3 | R.APFC-1 | 0.29, 0.081, 0.486 [-0.04 0.57] |
| N2R4 | L.SPC | −0.03, 0.862, 2.547 [-0.34 0.29] |
| N2R5 | R.SPC | −0.12, 0.482, 2.410 [-0.43 0.21] |
| ***N3: SN*** | | |
| N3R1 | DACC | −0.05, 0.765, 3.060 [-0.37 0.28] |
| N3R2 | L.APFC-2 | −0.02, 0.886, 1.724 [-0.34 0.29] |
| N3R3 | R.APFC-2 | 0.70, **0.000***, **0.00**** [0.48 0.83] |
| N3R4 | L.I | 0.41, **0.011***, 0.077 [0.10 0.65] |
| N3R5 | R.I | 0.03, 0.849, 3.060 [-0.29 0.35] |
| N3R6 | L.LPC-2 | 0.56, **0.0002***, **0.002**** [0.30 0.75] |
| N3R7 | R.LPC-2 | 0.61, **0.000***, **0.00**** [0.37 0.78] |

*significant at $p \leq 0.05$.
**significant at $p1 \leq 0.05$ (adjusted p-values after Bonferroni-Holm correction).
[CI] represents confidence intervals at 95% level.

suggested that the association between negatively valenced mood states and subjective sleepiness could be due to the fact that SD is typically not a pleasant experience, and both experiences (sleepiness due to SD and negative mood due to SD) could lead to similar subjective unpleasant sensations (Franzen et al., 2008). Overall, the present findings suggest that greater compactness of WM for most of the ROIs within the triple network model (DMN, CEN and SN) is associated with better ability to sustain positive mood when lacking sleep. However, to our knowledge, this is the first study to use QA as a WM metric to predict responses to SD, therefore the validity of these neural mechanisms and their role in the association between mood and SD is yet to be confirmed.

## 5. Limitations and future directions

Our findings should be interpreted in consideration of the following limitations. First, this study involved diffusion-weighted data based on anisotropic voxel dimensions, and neuroanatomical data of moderate resolution. Additionally, diffusion measures such as those used here are subject to many factors that may affect interpretation, including myelination, crossing fibers, axonal deterioration, viscosity, and extracellular factors that may hinder diffusion, just to name a few. Thus, while we interpret our findings as evidence of differences in axonal pathways, other interpretations are possible. Future studies would benefit from the use of more advanced high-resolution diffusion-weighted and anatomical scans. Second, our study focused on only structural characteristics of the triple-network model and their association with mood-shifts. It would be of importance for future work to identify and clarify the causal associations between mood variability and whole-brain functional characteristics, *especially* large-scale effective connectivity measures. Although using whole-brain effective connectivity techniques could be challenging, recent developments in this domain, such as the spectral dynamic causal modeling approach (Friston et al., 2014), in conjunction with structural connectivity constraints, could be used to investigate more complex associations between mood sustainment and brain connectivity following sleep loss than have been possible with previous techniques.

## 6. Conclusions

Greater compactness of WM, as reflected by greater anisotropic WM water density, of specific regions within the triple-network model, are significantly associated with individual differences in the ability to sustain mood during an overnight period of SD. However, none of the GM morphometry measures used here played a significant role in modulating mood following SD. Our findings suggest that individuals with more resilience to mood degradation following SD show evidence of more compact region-specific WM. However, a significant amount of work still remains to be done to establish more reliable structural neural biomarkers of mood vulnerability following sleep loss. In addition, future research should also focus on more advanced functional analysis techniques in terms of large-scale effective brain connectivity to further confirm the role of triple-network model and individual differences in positive and negative mood states separately.

## Data and code availability statement

Any data and code associated with this article will be made available by reasonable request to senior author (WDSK).

## Disclosure statement

None.

## Acknowledgements

This study was supported by Defense Advanced Research Projects Agency (DARPA) (DARPA Young Faculty Award D12AP0024 to WDSK). We would like to thank Mareen Weber, Elisabeth Olson, Christian Webb, Maia Kipman, Sophie DelDonno, Zack Schwab, Lily (Preer) Sonis, Hanna Gogel, Olga Tkachenko, and David Penetar for their contribution to data collection.

## Appendix A. Supplementary data

Supplementary data to this article can be found online at https://doi.org/10.1016/j.neuroimage.2019.116123.

## References

Batchelor, P.G., Castellano Smith, A.D., Hill, D.L., Hawkes, D.J., Cox, T.C., Dean, A.F., 2002. Measures of folding applied to the development of the human fetal brain. IEEE Trans. Med. Imaging 21 (8), 953–965. https://doi.org/10.1109/TMI.2002.803108. PubMed PMID: 12472268.

Beattie, L., Kyle, S.D., Espie, C.A., Biello, S.M., 2015. Social interactions, emotion and sleep: a systematic review and research agenda. Sleep Med. Rev. 24, 83–100. https://doi.org/10.1016/j.smrv.2014.12.005. PubMed PMID: 25697832.

Beaulieu, C., 2002. The basis of anisotropic water diffusion in the nervous system - a technical review. NMR Biomed. 15 (7–8), 435–455. https://doi.org/10.1002/nbm.782. PubMed PMID: 12489094.

Ben Simon, E., Maron-Katz, A., Lahav, N., Shamir, R., Hendler, T., 2017. Tired and misconnected: a breakdown of brain modularity following sleep deprivation. Hum. Brain Mapp. 38 (6), 3300–3314. https://doi.org/10.1002/hbm.23596. PubMed PMID: 28370703.

Caldwell, J.A., Mu, Q., Smith, J.K., Mishory, A., Caldwell, J.L., Peters, G., et al., 2005. Are individual differences in fatigue vulnerability related to baseline differences in cortical activation? Behav. Neurosci. 119 (3), 694–707. https://doi.org/10.1037/0735-7044.119.3.694. PubMed PMID: 15998190.

Chee, M.W., Tan, J.C., 2010. Lapsing when sleep deprived: neural activation characteristics of resistant and vulnerable individuals. Neuroimage 51 (2), 835–843. https://doi.org/10.1016/j.neuroimage.2010.02.031. PubMed PMID: 20171288.

Chen, W.H., Chen, J., Lin, X., Li, P., Shi, L., Liu, J.J., et al., 2018. Dissociable effects of sleep deprivation on functional connectivity in the dorsal and ventral default mode networks. Sleep Med. 50, 137–144. https://doi.org/10.1016/j.sleep.2018.05.040. PubMed PMID: 30055480.

Cui, J., Tkachenko, O., Gogel, H., Kipman, M., Preer, L.A., Weber, M., et al., 2015. Microstructure of frontoparietal connections predicts individual resistance to sleep deprivation. Neuroimage 106, 123–133. https://doi.org/10.1016/j.neuroimage.2014.11.035. PubMed PMID: 25463450.

De Havas, J.A., Parimal, S., Soon, C.S., Chee, M.W., 2012. Sleep deprivation reduces default mode network connectivity and anti-correlation during rest and task performance. Neuroimage 59 (2), 1745–1751. https://doi.org/10.1016/j.neuroimage.2011.08.026. PubMed PMID: 21872664.

Dennis, L.E., Wohl, R.J., Selame, L.A., Goel, N., 2017. Healthy adults display long-term trait-like neurobehavioral resilience and vulnerability to sleep loss. Sci. Rep. 7 (1), 14889. https://doi.org/10.1038/s41598-017-14006-7. PubMed PMID: 29097703; PubMed Central PMCID: PMCPMC5668275.

Deppe, M., Marinell, J., Kramer, J., Duning, T., Ruck, T., Simon, O.J., et al., 2014. Increased cortical curvature reflects white matter atrophy in individual patients with

early multiple sclerosis. Neuroimage Clin. 6, 475–487. https://doi.org/10.1016/j.nicl.2014.02.012. PubMed PMID: 25610761; PubMed Central PMCID: PMCPMC4299934.
Desikan, R.S., Segonne, F., Fischl, B., Quinn, B.T., Dickerson, B.C., Blacker, D., et al., 2006. An automated labeling system for subdividing the human cerebral cortex on MRI scans into gyral based regions of interest. Neuroimage 31 (3), 968–980. https://doi.org/10.1016/j.neuroimage.2006.01.021. PubMed PMID: 16530430.
Drummond, S.P., Brown, G.G., Gillin, J.C., Stricker, J.L., Wong, E.C., Buxton, R.B., 2000. Altered brain response to verbal learning following sleep deprivation. Nature 403 (6770), 655–657. https://doi.org/10.1038/35001068. PubMed PMID: 10688201.
Durmer, J.S., Dinges, D.F., 2005. Neurocognitive consequences of sleep deprivation. Semin. Neurol. 25 (1), 117–129. PubMed PMID: 15798944.
Feng, P., Becker, B., Zheng, Y., Feng, T., 2018. Sleep deprivation affects fear memory consolidation: bi-stable amygdala connectivity with insula and ventromedial prefrontal cortex. Soc. Cogn. Affect. Neurosci. 13 (2), 145–155. https://doi.org/10.1093/scan/nsx148. PubMed PMID: 29272546; PubMed Central PMCID: PMCPMC5827342.
Fischl, B., Dale, A.M., 2000. Measuring the thickness of the human cerebral cortex from magnetic resonance images. Proc. Natl. Acad. Sci. U. S. A. 97 (20), 11050–11055. https://doi.org/10.1073/pnas.200033797. PubMed PMID: 10984517; PubMed Central PMCID: PMCPMC27146.
Fischl, B., Sereno, M.I., Dale, A.M., 1999. Cortical surface-based analysis. II: inflation, flattening, and a surface-based coordinate system. Neuroimage 9 (2), 195–207. https://doi.org/10.1006/nimg.1998.0396. PubMed PMID: 9931269.
Folstein, M.F., Luria, R., 1973. Reliability, validity, and clinical application of the visual analogue mood scale. Psychol. Med. 3 (4), 479–486. Epub 1973/11/01. PubMed PMID: 4762224.
Franzen, P.L., Siegle, G.J., Buysse, D.J., 2008. Relationships between affect, vigilance, and sleepiness following sleep deprivation. J. Sleep Res. 17 (1), 34–41. https://doi.org/10.1111/j.1365-2869.2008.00635.x. PubMed PMID: WOS:000253719600008.
Friston, K.J., Kahan, J., Biswal, B., Razi, A., 2014. A DCM for resting state fMRI. Neuroimage 94, 396–407. https://doi.org/10.1016/j.neuroimage.2013.12.009. PubMed PMID: 24345387; PubMed Central PMCID: PMCPMC4073651.
Goldstein, A.N., Walker, M.P., 2014. The role of sleep in emotional brain function. Annu. Rev. Clin. Psychol. 10, 679–708. https://doi.org/10.1146/annurev-clinpsy-032813-153716. PubMed PMID: 24499013; PubMed Central PMCID: PMCPMC4286245.
Habas, C., Kamdar, N., Nguyen, D., Prater, K., Beckmann, C.F., Menon, V., et al., 2009. Distinct cerebellar contributions to intrinsic connectivity networks. J. Neurosci. 29 (26), 8586–8594. https://doi.org/10.1523/Jneurosci.1868-09.2009. PubMed PMID: WOS:000267613400030.
Hogstrom, L.J., Westlye, L.T., Walhovd, K.B., Fjell, A.M., 2013. The structure of the cerebral cortex across adult life: age-related patterns of surface area, thickness, and gyrification. Cerebr. Cortex 23 (11), 2521–2530. https://doi.org/10.1093/cercor/bhs231. PubMed PMID: 22892423.
Horne, J.A., Ostberg, O., 1976. A self-assessment questionnaire to determine morningness-eveningness in human circadian rhythms. Int. J. Chronobiol. 4 (2), 97–110. PubMed PMID: 1027738.
Im, K., Lee, J.M., Lyttelton, O., Kim, S.H., Evans, A.C., Kim, S.I., 2008. Brain size and cortical structure in the adult human brain. Cerebr. Cortex 18 (9), 2181–2191. https://doi.org/10.1093/cercor/bhm244. PubMed PMID: 18234686.
Jack, J.J.B., Noble, D., Tsien, R.W., 1983. Electric Current Flow in Excitable Cells. Oxford University Press.
Kahn-Greene, E.T., Lipizzi, E.L., Conrad, A.K., Kamimori, G.H., Killgore, W.D.S., 2006. Sleep deprivation adversely affects interpersonal responses to frustration. Personal. Individ. Differ. 41, 1433–1443.
Killgore, W.D., 2010. Effects of sleep deprivation on cognition. Prog. Brain Res. 185, 105–129. https://doi.org/10.1016/B978-0-444-53702-7.00007-5. PubMed PMID: 21075236.
Killgore, W.D., 2013. Self-reported sleep correlates with prefrontal-amygdala functional connectivity and emotional functioning. Sleep 36 (11), 1597–1608. https://doi.org/10.5665/sleep.3106. PubMed PMID: 24179291; PubMed Central PMCID: PMCPMC3792375.
Killgore, W.D.S., Kahn-Greene, E.T., Lipizzi, E.L., Newman, R.A., Kamimori, G.H., Balkin, T.J., 2008. Sleep deprivation reduces perceived emotional intelligence and constructive thinking skills. Sleep Med. 9 (5), 517–526. https://doi.org/10.1016/j.sleep.2007.07.003. PubMed PMID: 17765011.
Killgore, W.D.S., Schwab, Z.J., Weiner, M.R., 2012. Self-reported nocturnal sleep duration is associated with next-day resting state functional connectivity. Neuroreport 23 (13), 741–745. https://doi.org/10.1097/WNR.0b013e3283565056. Epub 2012/08/09, PubMed PMID: 22872066.
Killgore, W.D.S., Weber, M., 2014. Sleep deprivation and cognitive performance. In: Bianchi, M.T. (Ed.), Sleep Deprivation and Disease: Effects on the Body, Brain and Behavior. Springer, New York.
King, A.C., Belenky, G., Van Dongen, H.P., 2009. Performance impairment consequent to sleep loss: determinants of resistance and susceptibility. Curr. Opin. Pulm. Med. 15 (6), 559–564. https://doi.org/10.1097/MCP.0b013e3283319aad. PubMed PMID: 19713847.
Luo, Y., Kong, F., Qi, S., You, X., Huang, X., 2016. Resting-state functional connectivity of the default mode network associated with happiness. Soc. Cogn. Affect. Neurosci. 11 (3), 516–524. https://doi.org/10.1093/scan/nsv132. PubMed PMID: 26500289; PubMed Central PMCID: PMCPMC4769634.
Menon, V., 2011. Large-scale brain networks and psychopathology: a unifying triple network model. Trends Cogn. Sci. 15 (10), 483–506. https://doi.org/10.1016/j.tics.2011.08.003. PubMed PMID: WOS:000295662800008.
Monk, T.H., 1989. A Visual Analogue Scale technique to measure global vigor and affect. Psychiatry Res. 27 (1), 89–99. Epub 1989/01/01. PubMed PMID: 2922449.
Motomura, Y., Katsunuma, R., Yoshimura, M., Mishima, K., 2017. Two days' sleep debt causes mood decline during resting state via diminished amygdala-prefrontal connectivity. Sleep 40 (10). https://doi.org/10.1093/sleep/zsx133. PubMed PMID: 28977527.
Patanaik, A., Zagorodnov, V., Kwoh, C.K., Chee, M.W., 2014. Predicting vulnerability to sleep deprivation using diffusion model parameters. J. Sleep Res. 23 (5), 576–584. https://doi.org/10.1111/jsr.12166. PubMed PMID: 24861212.
Penetar, D., McCann, U., Thorne, D., Kamimori, G., Galinski, C., Sing, H., et al., 1993. Caffeine reversal of sleep deprivation effects on alertness and mood. Psychopharmacology (Berlin) 112 (2–3), 359–365. PubMed PMID: 7871042.
Raichle, M.E., 2011. The restless brain. Brain Connect. 1 (1), 3–12. https://doi.org/10.1089/brain.2011.0019. PubMed PMID: 22432951; PubMed Central PMCID: PMCPMC3621343.
Razi, A., Seghier, M.L., Zhou, Y., McColgan, P., Zeidman, P., Park, H.J., et al., 2017. Large-scale DCMs for resting-state fMRI. Netw. Neurosci. 1 (3), 222–241. https://doi.org/10.1162/netn_a_00015. PubMed PMID: WOS:000449588600002.
Rocklage, M., Williams, V., Pacheco, J., Schnyer, D.M., 2009. White matter differences predict cognitive vulnerability to sleep deprivation. Sleep 32 (8), 1100–1103. PubMed PMID: 19725262; PubMed Central PMCID: PMCPMC2717201.
Ronan, L., Voets, N.L., Hough, M., Mackay, C., Roberts, N., Suckling, J., et al., 2012. Consistency and interpretation of changes in millimeter-scale cortical intrinsic curvature across three independent datasets in schizophrenia. Neuroimage 63 (1), 611–621. https://doi.org/10.1016/j.neuroimage.2012.06.034. PubMed PMID: WOS:000308770300062.
Rorden, C., Karnath, H.O., Bonilha, L., 2007. Improving lesion-symptom mapping. J. Cogn. Neurosci. 19 (7), 1081–1088. https://doi.org/10.1162/jocn.2007.19.7.1081. PubMed PMID: 17583985.
Rupp, T.L., Wesensten, N.J., Balkin, T.J., 2012. Trait-like vulnerability to total and partial sleep loss. Sleep 35 (8), 1163–1172. https://doi.org/10.5665/sleep.2010. PubMed PMID: 22851812; PubMed Central PMCID: PMCPMC3397820.
Schwarz, J., Axelsson, J., Gerhardsson, A., Tamm, S., Fischer, H., Kecklund, G., et al., 2018. Mood impairment is stronger in young than in older adults after sleep deprivation. J. Sleep Res., e12801 https://doi.org/10.1111/jsr.12801. PubMed PMID: 30585371.
Seeley, W.W., Menon, V., Schatzberg, A.F., Keller, J., Glover, G.H., Kenna, H., et al., 2007. Dissociable intrinsic connectivity networks for salience processing and executive control. J. Neurosci. 27 (9), 2349–2356. https://doi.org/10.1523/Jneurosci.5587-06.2007. PubMed PMID: WOS:000244758500023.
Shao, Y., Lei, Y., Wang, L., Zhai, T., Jin, X., Ni, W., et al., 2014. Altered resting-state amygdala functional connectivity after 36 hours of total sleep deprivation. PLoS One 9 (11), e112222. https://doi.org/10.1371/journal.pone.0112222. PubMed PMID: 25372882; PubMed Central PMCID: PMCPMC4221616.
Sheehan, D.V., Lecrubier, Y., Sheehan, K.H., Amorim, P., Janavs, J., Weiller, E., et al., 1998. The Mini-International Neuropsychiatric Interview (M.I.N.I.): the development and validation of a structured diagnostic psychiatric interview for DSM-IV and ICD-10. J. Clin. Psychiatry 59 (Suppl. 20), 22–33 quiz 4-57. PubMed PMID: 9881538.
Simon, E.B., Oren, N., Sharon, H., Kirschner, A., Goldway, N., Okon-Singer, H., et al., 2015. Losing neutrality: the neural basis of impaired emotional control without sleep. J. Neurosci. 35 (38), 13194–13205. https://doi.org/10.1523/JNEUROSCI.1314-15.2015. PubMed PMID: 26400948.
Stern, R.A., Arruda, J.E., Hooper, C.R., Wolfner, G.D., Morey, C.E., 1997. Visual analogue mood scales to measure internal mood state in neurologically impaired patients: description and initial validity evidence. Aphasiology 11 (1), 59–71. https://doi.org/10.1080/02687039708248455.
Taruffi, L., Pehrs, C., Skouras, S., Koelsch, S., 2017. Effects of sad and happy music on mind-wandering and the default mode network. Sci. Rep. 7 (1), 14396. https://doi.org/10.1038/s41598-017-14849-0. PubMed PMID: 29089542; PubMed Central PMCID: PMCPMC5663956.
Tempesta, D., Couyoumdjian, A., Curcio, G., Moroni, F., Marzano, C., De Gennaro, L., et al., 2010. Lack of sleep affects the evaluation of emotional stimuli. Brain Res. Bull. 82 (1–2), 104–108. https://doi.org/10.1016/j.brainresbull.2010.01.014. PubMed PMID: 20117179.
Tkachenko, O., Dinges, D.F., 2018. Interindividual variability in neurobehavioral response to sleep loss: a comprehensive review. Neurosci. Biobehav. Rev. 89, 29–48. https://doi.org/10.1016/j.neubiorev.2018.03.017. PubMed PMID: 29563066.
Tuch, D.S., Salat, D.H., Wisco, J.J., Zaleta, A.K., Hevelone, N.D., Rosas, H.D., 2005. Choice reaction time performance correlates with diffusion anisotropy in white matter pathways supporting visuospatial attention. Proc. Natl. Acad. Sci. U. S. A. 102 (34), 12212–12217. https://doi.org/10.1073/pnas.0407259102. PubMed PMID: WOS:000231476500046.
Van Dongen, H.P., Belenky, G., 2009. Individual differences in vulnerability to sleep loss in the work environment. Ind. Health 47 (5), 518–526. PubMed PMID: 19834261.
Van Dongen, H.P.A., Baynard, M.D., Maislin, G., Dinges, D.F., 2004. Systematic interindividual differences in neurobehavioral impairment from sleep loss: evidence of trait-like differential vulnerability. Sleep 27 (3), 423–433. PubMed PMID: WOS:000223169000011.
Van Dongen, H.P., Caldwell Jr., J.A., Caldwell, J.L., 2011. Individual differences in cognitive vulnerability to fatigue in the laboratory and in the workplace. Prog. Brain Res. 190, 145–153. https://doi.org/10.1016/B978-0-444-53817-8.00009-8. PubMed PMID: 21531250.
Van Dongen, H.P., Bender, A.M., Dinges, D.F., 2012. Systematic individual differences in sleep homeostatic and circadian rhythm contributions to neurobehavioral impairment during sleep deprivation. Accid. Anal. Prev. 45 (Suppl. l), 11–16. https://doi.org/10.1016/j.aap.2011.09.018. PubMed PMID: 22239924; PubMed Central PMCID: PMCPMC3260461.

Wesensten, N.J., Killgore, W.D.S., Balkin, T.J., 2005. Performance and alertness effects of caffeine, dextro amphetamine, and modafinil during sleep deprivation. J. Sleep Res. 14 (3), 255–266. https://doi.org/10.1111/j.1365-2869.2005.00468.x. PubMed PMID: WOS:000231853800006.

Winkler, A.M., Kochunov, P., Blangero, J., Almasy, L., Zilles, K., Fox, P.T., et al., 2010. Cortical thickness or grey matter volume? The importance of selecting the phenotype for imaging genetics studies. Neuroimage 53 (3), 1135–1146. https://doi.org/10.1016/j.neuroimage.2009.12.028. PubMed PMID: 20006715; PubMed Central PMCID: PMCPMC2891595.

Winkler, A.M., Greve, D.N., Bjuland, K.J., Nichols, T.E., Sabuncu, M.R., Håberg, A.K., et al., 2018. Joint analysis of cortical area and thickness as a replacement for the analysis of the volume of the cerebral cortex. Cerebr. Cortex 28 (2), 738–749. https://doi.org/10.1093/cercor/bhx308.

Yeh, F.C., Tseng, W.Y., 2011. NTU-90: a high angular resolution brain atlas constructed by q-space diffeomorphic reconstruction. Neuroimage 58 (1), 91–99.

Yeh, F.C., Verstynen, T.D., Wang, Y., Fernandez-Miranda, J.C., Tseng, W.Y., 2013. Deterministic diffusion fiber tracking improved by quantitative anisotropy. PLoS One 8 (11), e80713. https://doi.org/10.1371/journal.pone.0080713. PubMed PMID: 24348913; PubMed Central PMCID: PMCPMC3858183.

Yeh, F.C., Vettel, J.M., Singh, A., Poczos, B., Grafton, S.T., Erickson, K.I., et al., 2016. Quantifying differences and similarities in whole-brain white matter architecture using local connectome fingerprints. PLoS Comput. Biol. 12 (11), e1005203 https://doi.org/10.1371/journal.pcbi.1005203. Epub 2016/11/16, PubMed PMID: 27846212.

Yeh, F.C., Badre, D., Verstynen, T., 2016. Connectometry: a statistical approach harnessing the analytical potential of the local connectome. Neuroimage 125, 162–171. https://doi.org/10.1016/j.neuroimage.2015.10.053. Epub 2015/10/27, PubMed PMID: 26499808.

Yeo, B.T., Tandi, J., Chee, M.W., 2015. Functional connectivity during rested wakefulness predicts vulnerability to sleep deprivation. Neuroimage 111, 147–158. https://doi.org/10.1016/j.neuroimage.2015.02.018. PubMed PMID: 25700949.

Yoo, S.S., Gujar, N., Hu, P., Jolesz, F.A., Walker, M.P., 2007. The human emotional brain without sleep - a prefrontal amygdala disconnect. Curr. Biol. 17 (20), R877–R878. https://doi.org/10.1016/j.cub.2007.08.007. PubMed PMID: WOS:000250466400009.

Zielinski, M.R., McKenna, J.T., McCarley, R.W., 2016. Functions and mechanisms of sleep. AIMS Neurosci. 3 (1), 67–104. https://doi.org/10.3934/Neuroscience.2016.1.67. PubMed PMID: 28413828; PubMed Central PMCID: PMCPMC5390528.